Defence Science Journal, Vol. 75, No. 1, January 2025, pp. 3-9, DOI : 10.14429/dsj.19883

Aerodynamic Impacts of Convergent Slot Implementation on Hinged and Morphed NACA 0012 Airfoil Operating at a High Reynolds Number

Ravi Kumar and Santanu Ghosh*

Department of Aerospace Engineering, IIT Madras, Chennai – 600 036, India
**E-mail: sghosh1@smail.iitm.ac.in*

ABSTRACT

Trailing-edge modifications on the NACA 0012 airfoil for lift enhancement are numerically investigated at a Reynolds number 4.58×10^6. Specifically, three variations in the trailing-edge geometry are tested: a hinged flap with hinge location at 70 % of chord, and two variations of continuous camber-morphed trailing edge: from 70 % chord to 100 % chord and from 70 % chord to 90 % chord. Reynolds-Averaged Navier-Stokes (RANS) simulations are performed using ANSYS Fluent with Menter's SST *k-ω* two-equation turbulence model. Predictions of aerodynamic characteristics reveal that the continuous morphing of trailing edge enhances lift generation and improves aerodynamic efficiency compared to the hinged flap. Further, for an angle of attack of 10°, it is shown that boundary-layer separation is less for both camber-morphed trailing-edge configurations compared to hinged flap configuration. The introduction of a convergent slot just upstream of the hinge/start-of-morphing location results in the elimination of flow separation in all cases, and improved aerodynamic efficiency, especially for the hinged-flap configuration.

Keywords: Aerodynamic efficiency; RANS, Camber-morphed flap; Convergent slot; Flow separation

NOMENCLATURE

c	: Chord length
LE	: Leading edge
TE	: Trailing edge
M	: Mach number
Re	: Reynolds number
β	: Flap angle
k	: Turbulence kinetic energy
ω	: Specific rate of diffusion
b	: Trailing edge flap length
c_l	: Sectional coefficient of lift
c_d	: Sectional coefficient of drag
c_p	: Coefficient of pressure
$\varphi(x)$	: Polynomial expression for morphing surfaces
x/c	: Running distance in stream-wise direction
y/c	: Running distance in transverse direction

1. INTRODUCTION

Lift augmentation in wings can be achieved by using trailing-edge flaps, which effectively change the camber of the wing section discretely when the flap is deflected. An alternative to using flaps or discrete camber morphing is the application of continuous camber morphing near the trailing edge Daynes[1], *et al.* The concept of morphing in aircraft has been developed by observing the ability of insects and birds to change their wing shape during flight in a wide range of situations. Various morphing techniques include changing the camber of the wing section (airfoil) (Daynes[1], *et al.*), increasing the planform area (Skillen[2], *et al.*), bending (Lingling[3], *et al.*) and twisting (Aso[4], *et al.*) the wing in a lateral direction, etc. Parker[5], dealt with the problem of the narrow speed range of an airplane using camber morphing. Specifically, he increased the maximum speed by varying the camber of a wing surface using loads and thus presented the Parker variable wing configuration in a biplane or triplane aircraft. Spillman[6], *et al*. showed that using variable camber flaps on NACA 64012 at cruise conditions reduces drag by 23 %. Dhileep[7], *et al.* investigated the aerodynamic characteristics of NACA 0012 airfoil morphed using a Single Corrugated Variable-Camber (SCVC) morphing technique and found that in terms of aerodynamic efficiency and endurance factor morphing is beneficial for moderate to high lift requirements. Woods[8], *et al.* proposed the Fishbone Active Camber Concept (FishBAC) based on the Euler-Bernoulli beam theory for deformation, and it was found that the FishBAC airfoil has much lower drag and higher lift than a hinged flap airfoil. In the recent past, Kumar[9], *et al.* studied the combined effect of morphing and corrugation on the airfoil surface. It is found that corrugated camber-morphed airfoils are more efficient than the conventional hinged flap but less efficient than the smooth skin morphed airfoil for all sets of low to medium values of angles of attack when operated at high Reynolds number. Jawahar[10], *et al.* studied aerodynamic performance, pressure distribution, etc., for various trailing edge camber profiles applied to the NACA 0012 airfoil at different angles of attack at a moderate Reynolds number of 0.35 million. The authors reported improved aerodynamic performance with flow separation, which shifted downstream at higher angles of attack for the cambered flap.

Received : 06 February 2024, Revised : 06 August 2024
Accepted : 24 September 2024, Online published : 10 January 2025

For controlling flow separation and managing the boundary layer over the airfoils, numerous methods have been studied in the past. One of the passive methods considered is the use of slotted airfoils, which was first introduced to enhance the lifting characteristics of airplane wings by Parker[5] and Weick[11], *et al.* This method involves a slot that extends from the pressure side of the airfoil to the suction side. Due to the pressure difference between these sides, air flows through the slot, injecting momentum into the boundary layer on the suction side, thus improving aerodynamic performance. In the recent past, researchers Fawzi[12], *et al.* worked to enhance airfoil efficiency for applications in wind turbines, aircraft, propellers, and helicopters by using a slotted airfoil to overcome flow separation at high angles of attack. Numerical simulations with ANSYS Fluent showed that the optimised slotted design significantly increases the lift-to-drag ratio and delays stall, with the most effective slot configuration found at 60 % chord, 65° slope, and 1 % chord width. Whitman[13], *et al.* examined the impact of various configurations of the slot on the stall angle for an airfoil similar to the NACA 65(3)-618. Results show that slotted airfoils generate higher lift coefficients above 15º and lower drag coefficients at low angles of attack compared to a solid airfoil, with the small slotted airfoil performing best at high angles of attack. Beyhaghi[14], *et al.* introduced a narrow span-wise slot near the leading edge of a cambered airfoil to study its aerodynamic performance impact. Using NACA 4412 as the baseline and varying slot parameters at a Reynolds number of 1.6 million, CFD simulations and wind tunnel experiments show that optimal slot configurations can improve lift by up to 30 % with minimal drag penalty across various angles of attack.

This paper compares the aerodynamic performance of three different trailing-edge modifications: a discrete linear hinged flap with a hinge location at 0.7c and two variations of continuous trailing-edge camber-morphing that extend from 0.7*c* - 1.0*c* and from 0.7*c* - 0.9*c* on the NACA 0012 airfoil, for a Reynolds number of 4.58×10^6 and a fixed trailing-edge deflection of 10° using numerical simulations. The reason for using a continuous camber-morphing configuration that has the last 10 % of the chord unmorphed is due to the following: In general camber-morphing wing designs, the morphing is generally introduced in such a way that some portion of the airfoil trailing-edge is kept unmorphed Woods[8], *et al.* to ensure the structural integrity of the wing during the wide range of flight conditions.

Further, the effect of a slot (that connects the pressure side to the suction side of the airfoil) introduced just upstream of the hinged/morphed trailing edge is investigated. Specific attention is provided to the flow simulation with an angle of attack of 10º, which is typical for the take-off flight stage, wherein the deployment of the flaps is required for augmenting lift and lowering stall speeds.

2. METHODOLOGY

2.1 Model Setup & Computational Details

The baseline NACA 0012 airfoil coordinates are taken from the website www.airfoiltools.com. The airfoil with hinged flap has a hinge location at 0.7*c* and is constructed using the method as described in Jawahar[9], *et al.* The coordinates of the camber-morphed trailing edge, in which the morphing starts at 0.7*c*, are generated using a cubic polynomial, Eqn. (1-3), defined in Daynes[1], *et al.*

$$w(x) = \varphi(x)\sin(\beta) \tag{1}$$

$$\varphi(x) = 0\,; \qquad 0 \le x < c\text{-}b \tag{2}$$

$$= \frac{(c-x-b)^3}{b^2}\,; \qquad c\text{-}b \le x < c \tag{3}$$

where,

$w(x)$: Change in the baseline airfoil's y-coordinate

$\varphi(x)$: Cubic polynomial for morphing

β: Flap deflection angle in radians

x: Chord wise position

b: Trailing-edge flap length

c: Chord length

Figure 1(a) shows the trailing-edge geometry for the baseline NACA 0012 airfoil along with the trailing-edge modifications investigated in this work. For all the simulations presented in this work that involve trailing edge modification, either with a hinged-flap or camber morphing, a positive trailing edge deflection of 10º was considered. Reynolds-Averaged Navier-Stokes (RANS) simulations for flow at Re: 4.58×10^6 and M: 0.1969 are performed using ANSYS Fluent using the steady pressure-based solver with Menter's Shear Stress Transport (SST) *k-ω* turbulence model. Least squares cell-based gradient, and a second-order upwind scheme are used to discretize the viscous and inviscid terms in the momentum equations, whereas a first-order upwind scheme is employed to discretize turbulent kinetic energy and dissipation rate terms. A C-type domain has been used for the simulations (shown in Fig. 1(b) with boundary conditions indicated), and a 2-D structured mesh is generated for all the cases, as shown in Fig. 1(c), using commercially available grid generation software, Pointwise V17.3 R3. In the wall-normal direction (Fig. 1(d), the grid is stretched, with the y^+ value of the first node from the airfoil surface being less than unity for most of the airfoil length to resolve the laminar sub-layer.

2.2 Domain and Grid Convergence

Three sizes of the computational domain (10*c*, 30*c*, and 100*c*) are tested to check for domain size convergence, and it is found that the lift coefficient hardly changes when the domain size varied from 30*c* to 100*c*, as observed in Fig. 2(a). As such, a domain of 30*c* is considered for the study presented herein. A grid-convergence study (Fig. 2(b)) is performed for the baseline, hinged-flap, and the two variations of camber-morphed configurations with the number of grid nodes ranging from 8,660 to 562,080 and a mesh with 34,920 grid nodes was chosen. Also, a grid convergence test is performed (Fig. 2(c)) for the slotted configurations (slotted hinged, and slotted camber-morphed) trailing edge with the number of grid nodes ranging from 16,324 to 754,062 and a mesh with 55,567 grid nodes was determined to be sufficient. The grid resolution studies are shown for an angle of attack (α) of 10º. A grid was determined to have sufficient resolution for a particular case (baseline or with camber morphed trailing edge etc.) if further refinement of the grid did not produce any appreciable change

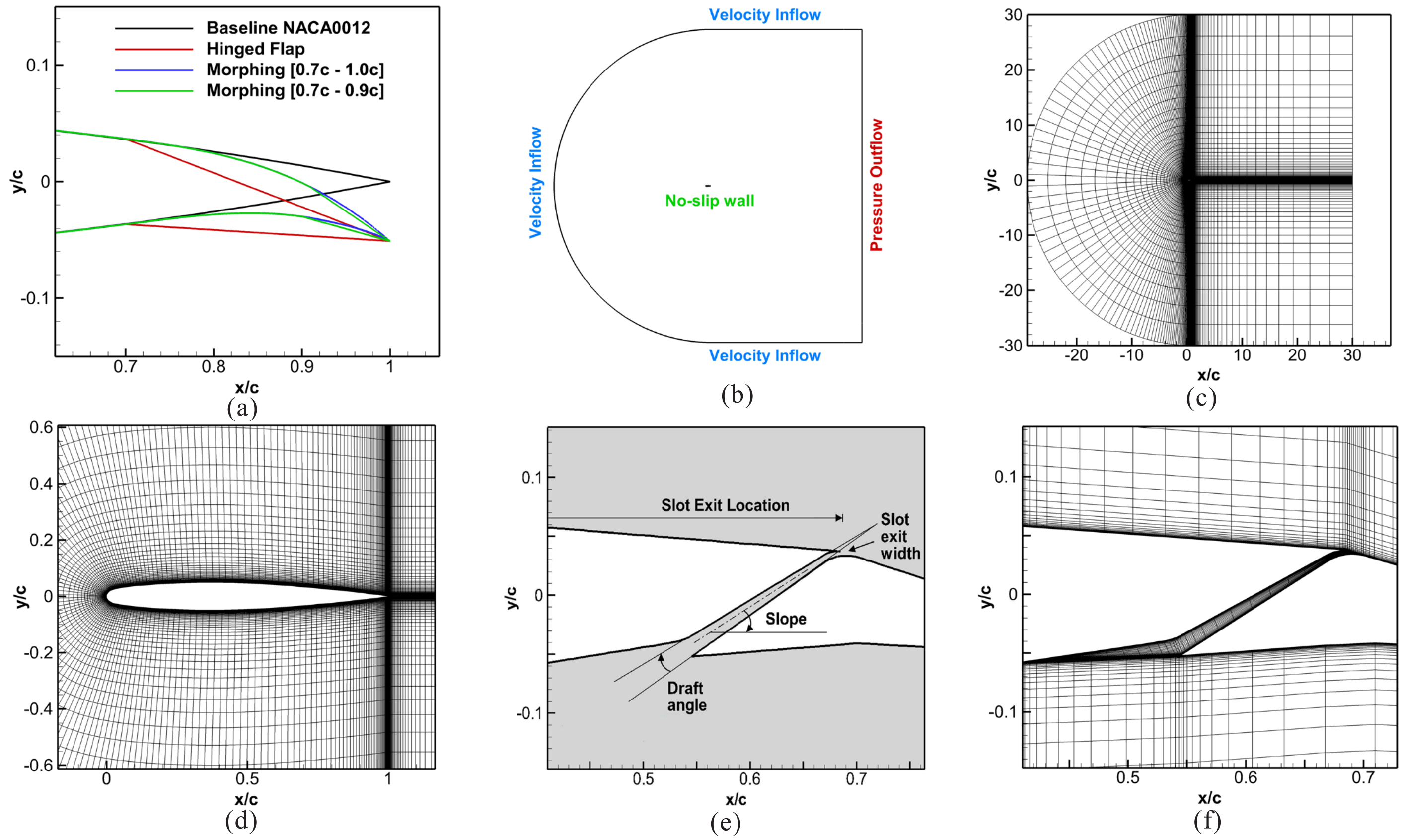

Figure 1. **(a) Trailing-edge geometry of baseline and other configurations of NACA 0012 airfoil (10° TE deflection for hinged and camber-morphed airfoils); (b) C-type domain used for the computations; Structured mesh for (c) Full domain, (d) Near the airfoil; (e) Geometry of the slot; and (f) Structured mesh in and around the slot. For clarity, alternate grid nodes are omitted.**

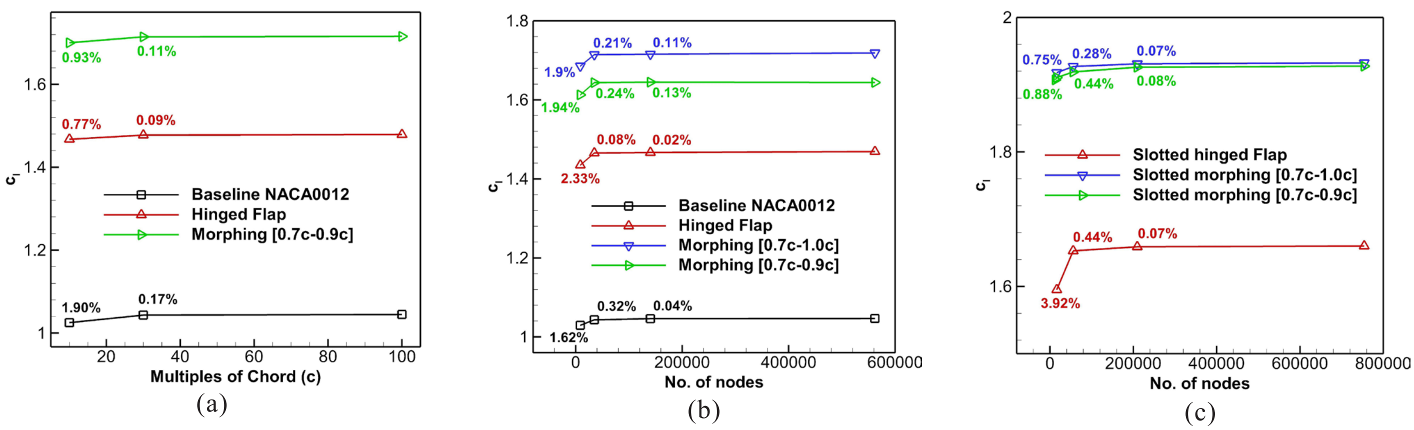

Figure 2. (a) Domain-size convergence test; Grid convergence tests for (b) Non-slotted airfoils and (c) Slotted airfoils.

(more than 5 %) in the lift coefficient. The percentage change in the c_l value compared to c_l of the most refined mesh is also illustrated in Fig. 2.

2.3 Slot Design

For finalising the contour of the converging type (non-linear) trailing edge slot for all three cases (hinged and two morphed configurations), a total of three parameters are considered: slope, draft angle, and slot exit width, as shown in Fig. 1(e). The different values of the parameters for which the slot effectiveness is checked for getting the maximum value of c_l are summarized in Table 1. On simulating the slot geometry for various combinations of the discrete values of the three parameters provided in the table below (a total of 80 cases), the best combination for the optimised geometry is determined to be 30°-4°-0.004c (written in the sequence: slope–draft angle–

Table 1. Parameters considered for the slot geometry optimisation

Parameters	Values
Slope	15°, 20°, 25°, 30° and 35°
Draft angle	2°, 4°, 6° and 8°
Slot exit width	(0.003*c*, 0.004*c*, 0.005*c*, 0.006*c*)
Slot exit location	0.7*c* (Fixed)

slot exit width). The "best" values of the parameters are found by varying only one parameter at a time.

For all these cases, the slot exit location is set at 0.7*c*, which corresponds to the root location of the hinged flap/camber-morphed trailing edge. The entry and the exit geometry of the slot were kept smooth to avoid flow separation at those locations. Fig. 1(e) shows the optimised slot geometry and Fig. 1(f) shows the structured mesh in and around the slot.

A convergent slot is chosen so that the flow accelerates through the slot while exiting (like a nozzle working at subsonic flow regime) tangentially to the suction surface and energizes the near-surface flow on the upper airfoil surface downstream

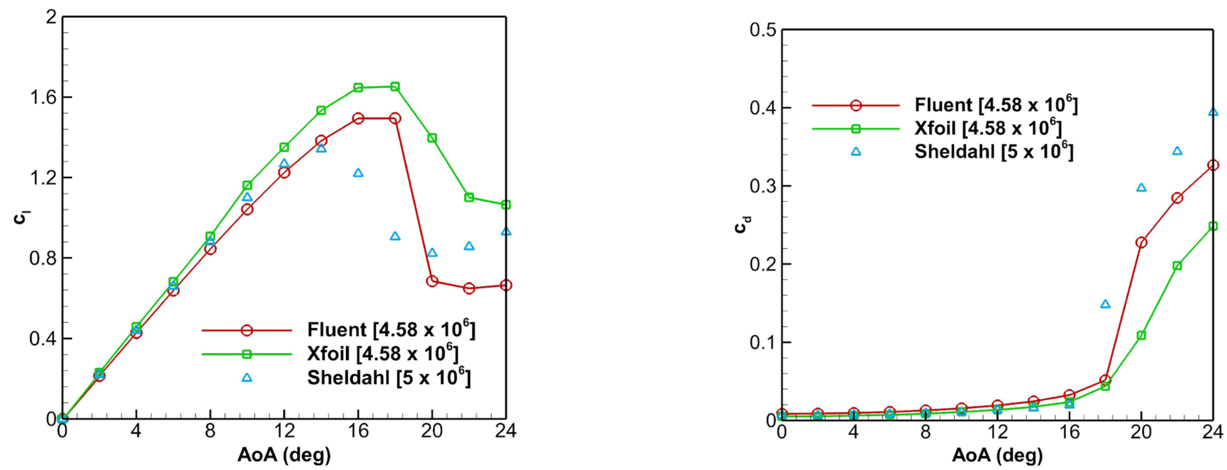

(a) (b)

Figure 3. c_l and c_d comparisons of Fluent with Xfoil predictions at Re: 4.58 × 10⁶ and experimental data at Re: 5×10⁶ (Sheldahl[15], *et al.*).

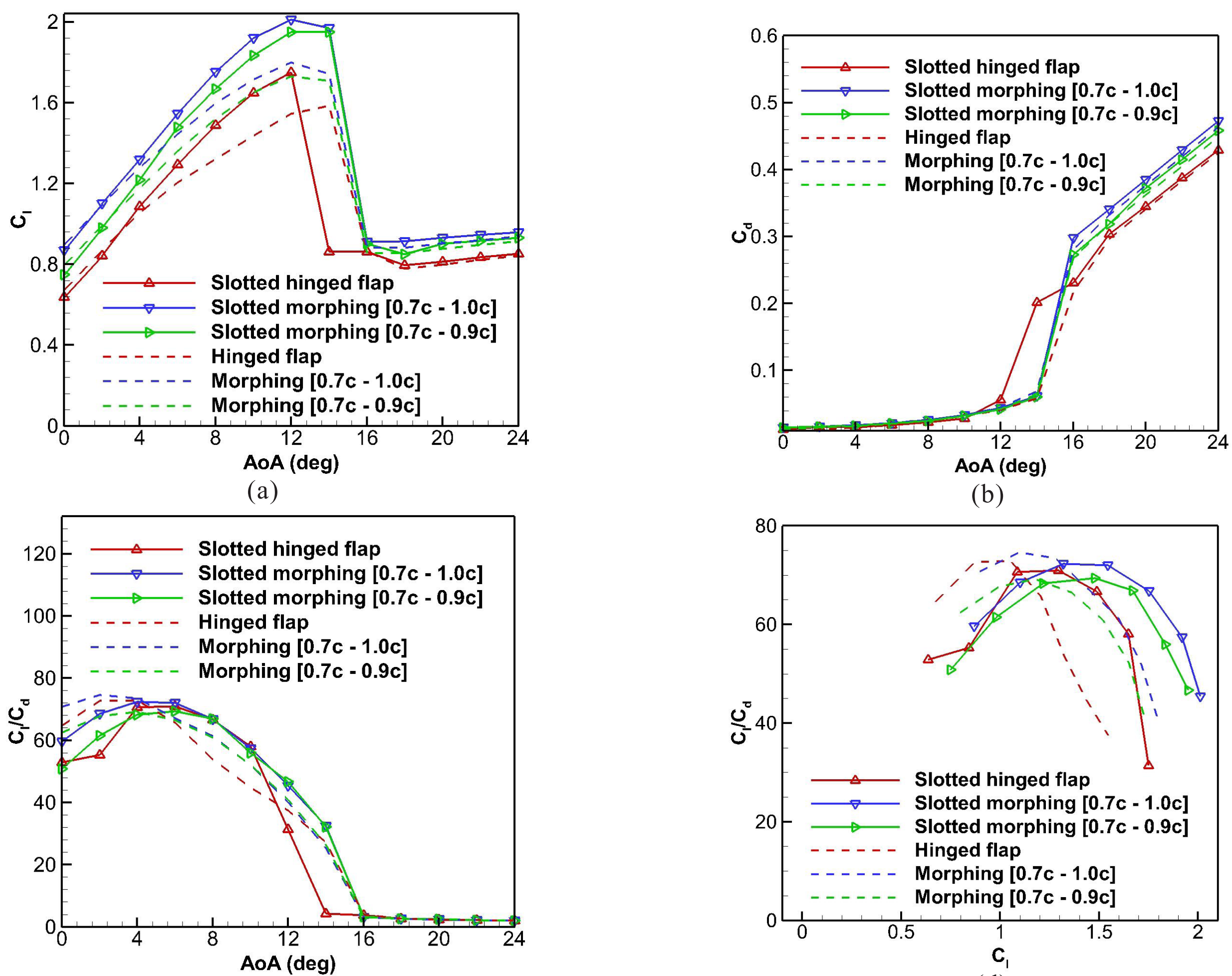

(a) (b)

(c) (d)

Figure 4. (a) c_l vs α; (b) c_d vs α; (c) c_l/c_d vs α and (d) c_l/c_d vs c_l comparisons among the slotted hinged and slotted camber-morphed airfoils.

Table 2. Comparison of lift (c_l), drag (c_d), and their ratios (c_l/c_d) for airfoils with different trailing-edge shapes with a slot (α: 10°); the change in values from the no-slotted cases are also included in parenthesis for reference

	Baseline NACA 0012	Hinged flap	Camber-morphed [0.7*c*-1.0*c*]	Camber-morphed [0.7*c*-0.9*c*]	Slotted hinged flap	Slotted camber-morphed [0.7*c*-1.0*c*]	Slotted camber-morphed [0.7*c*-0.9*c*]
c_l	1.04	1.43	1.71	1.65	1.65 (+0.22)	1.92 (+0.21)	1.83 (0.18)
c_d	0.0144	0.0321	0.0330	0.0316	0.0285 (-0.0036)	0.0334 (+0.0004)	0.0328 (+0.0012)
c_l/c_d	72.5	44.72	51.95	52.24	57.95 (+8.23)	57.38 (+5.53)	55.96 (+3.72)

of the slot that can help to delay/eliminate the flow separation near the airfoil trailing edge.

3. RESULTS AND DISCUSSION

3.1 Validation

For validating the computational setup, numerical predictions of lift (c_l) and drag coefficients (c_d) of the baseline NACA 0012 airfoil are compared with results from Xfoil and experimental data reported in the work by Sheldahl[15], *et al.* It can be observed from Fig. 3(a) and 3(b) that the present computations are in fair agreement with the result from Xfoil and literature until the stall is reached. Further, for angles of attack post-stall, the CFD predictions are observed to be closer to the experimental data. However, at low to moderate angles of attack, higher drag is predicted by the CFD computations compared to both Xfoil predictions and the experimental data[15]. This can be due to the fact that flow transition is not accounted for in the present computations.

3.2 Aerodynamic Performance

For the case of non-slotted airfoils, as observed in Fig. 4(a) and Table 2, the coefficient of lift (c_l) is enhanced by the introduction of a hinged flap (having a flap deflection of 10°) in the baseline airfoil. This is expected as the flap increases the effective camber of the airfoil. Compared to the hinged flap configuration, however, the camber-morphed airfoils (having a flap deflection of 10°) generate higher lift values for all the angles of attack (α). The camber-morphed [0.7*c*-1.0*c*] configuration is seen to generate slightly higher lift values than the camber-morphed [0.7*c* -0.9*c*] configuration. The coefficient of drag (c_d) values (Fig. 4(b)) with the trailing-edge modifications is also higher than that for baseline airfoil, which is expected as the trailing edge modifications introduce an effective camber. Minor differences, if any, are only observed in the predicted drag coefficients among the airfoils with trailing edge modifications at least still, the airfoil stalls.

From Fig. 4(c), observation can be made that the aerodynamic efficiency (c_l/c_d) of the hinged-flap airfoil lies between the smooth morphed [0.7*c* - 1.0*c*] and the smooth morphed [0.7*c* - 0.9*c*] configurations at low angles of attack ($\alpha < 6°$). However, at higher angles of attack, the airfoils with smooth morphed trailing edges perform better than the hinged-flap configuration.

It can also be observed that the maximum value of (c_l/c_d) does not change appreciably with trailing edge deflection. Fig. 4(d) shows the comparison of aerodynamic performance (c_l/c_d) with respect to lift coefficient (c_l) among all the airfoils. It can be seen that for high values of the lift coefficient (c_l>1.2), the airfoils with smoothly morphed trailing edge perform much better than the airfoil with hinged trailing edge flap. The lift augmentation achieved with the trailing edge deflections (hinged flap or camber morphing) compared to the baseline airfoil is also clear from this plot. When comparing with the slotted airfoils, it can be observed from Figs. 4(a), 4(c), and Table 2, that the introduction of the slot resulted in improvements in c_l and c_l/c_d when compared to the non-slotted cases.

For the angle of attack (α) less than 10°, no perceptible change in c_d is observed in Fig. 4(b) when compared to the corresponding non-slotted configurations. However, from Table 2, it is evident that while the drag increases slightly with the introduction of the slot for the smooth morphed trailing edges, it drops for the hinged-flap trailing edge configuration. The stall angle remains unchanged for both the morphed trailing edge configurations: [0.7*c*-1.0*c*] and [0.7*c*-0.9*c*].

3.3 Pressure Distribution

To further investigate the reason for the difference in the lift generated by the different non-slotted trailing-edge configurations, the c_p plot at an angle of attack (α) of 10° is plotted in Fig. 5(a). It can be observed from the plot that for the airfoil portion aft of the hinge location, i.e., $x/c \geq 0.7$, c_p values for the camber-morphed flaps are higher than for the hinged flap airfoil on the pressure surface, and lower on the suction surface, which results in generation of higher normal force and consequently higher lift. This clearly suggests that camber-morphing enhances lift compared to a hinged flap.

Also, from the plot, it can be observed that the pressure recovery on the suction surface of camber-morphed airfoils happens further downstream compared to the hinged flap case, which is expected to delay flow separation on the suction side. The c_p plot for the slotted configurations shown in Fig. 5(b) indicates that c_p values between the upper (suction) and the lower (pressure) airfoil surfaces for the slotted airfoil cases have increased for all the three modifications aft of the slot as compared with non-slot cases (Fig. 5(a)). This explains the generation of the higher lift values for this case compared to the non-slot configurations.

3.4 Flow near the trailing-edge

As observed in Fig. 6, lift-augmentation with a hinged-flap (Fig. 6(a)) or continuous camber morphing (Fig. 6(b)

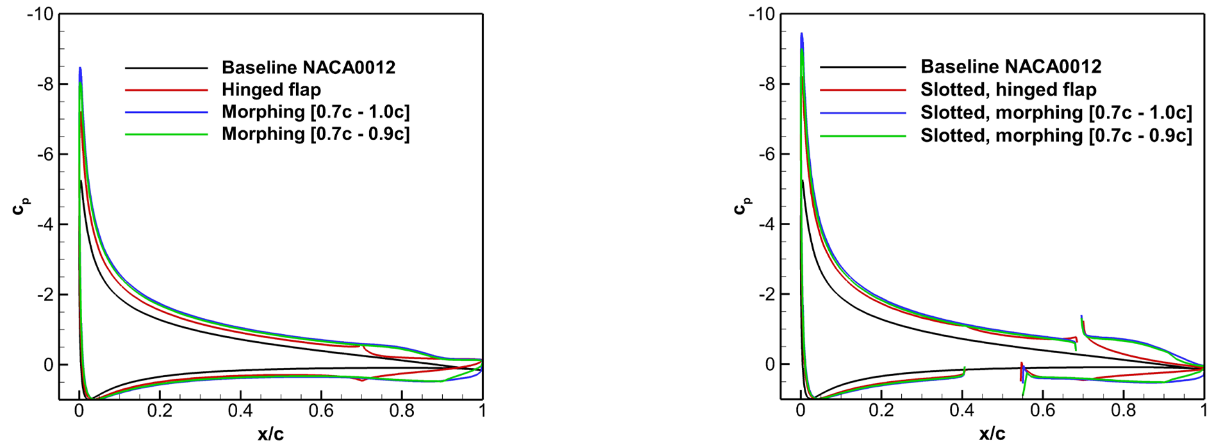

Figure 5: c_p comparison for (a) non-slotted and (b) slotted airfoil configurations (α: 10°).

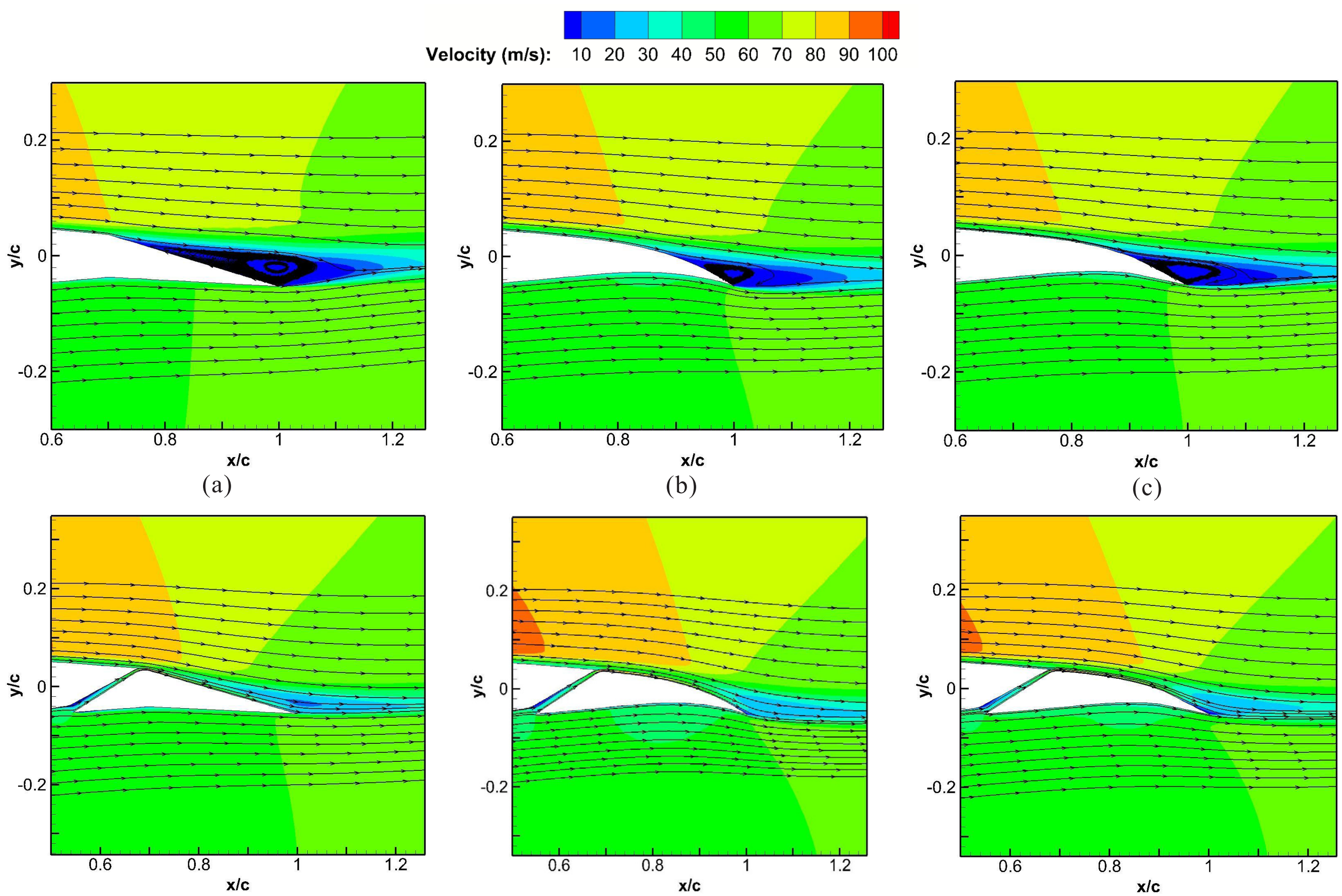

Figure 6. Velocity contours with streamlines for non-slotted airfoils (a) to (c) and for slotted airfoils (d) to (f) with different trailing edge modifications (α: 10°). (a) Hinged flap; (b) Camber-morphing [0.7c-1.0c]; (c) Camber-morphing [0.7*c*-0.9*c*]; (d) Slotted hinged flap TE; (e) Slotted camber-morphing [0.7*c*-1.0*c*]; (f) Slotted camber-morphing [0.7*c*-0.9*c*].

and Fig. 6(c)) of the trailing edge results in flow separation near the trailing edge at α: 10°. In order to investigate whether boundary-layer blowing can nullify the separation and improve the aerodynamic performance of the airfoil with trailing edge deflection, a convergent slot (as discussed in Section 2.3) is introduced just upstream of the start of the hinge/morphing location. With the introduction of a slot, which acts as a flow-separation passive control method for all the three modifications of the airfoil trailing edge, the flow separation is seen to be fully eliminated at the trailing edge as observed in Fig. 6(d), Fig. 6(e) and Fig. 6(f). The contours shown are presented for an angle of attack (α) of 10°.

4. CONCLUSION

Numerical investigations of flow past NACA 0012 airfoil are presented in this work that compare the efficacy of continuous camber-morphing (of the trailing edge) to a hinged flap at a high Reynolds number of 4.58 million. Results show that smooth camber-morphing of the trailing edge results in higher lift and (in most cases) better lift-to-drag ratios compared to the use of a hinged flap. Further, investigation of flow streamlines near the trailing edge at an angle-of-attack of 10^{o}, which is a typical value for aircraft take-off, reveal that flow separation is less with the use of continuous camber morphing than with the use of a hinged flap. Both effects are more pronounced when the morphing is carried out from 70 % of the chord all the way to the trailing edge. With the introduction of a convergent non-linear slot whose exit is fixed near the hinge/start-of-morphing location for both hinged and morphed trailing-edge configurations of the NACA 0012 airfoil, flow separation is eliminated, and lift generation is enhanced. The study shows that continuous camber morphing has the potential to improve aerodynamic performance during take-off/landing at high Reynolds number, which can be of interest for the passenger aircraft industry and large UAVs.

REFERENCES

1. Daynes, S. & Weaver, P.M. A morphing trailing edge device for a wind turbine. *J. Intelligent Material Syst.*, 2012, **23**(6). doi:10.1177/1045389X12438622
2. Skillen, M.D. & Crossley, W.A. Morphing wing weight predictors and their application in a template-based morphing aircraft sizing environment II. NACA Report No. 20080009778. February 2009.
3. Chu, L.; Li Q.; Gu F.; Du X.; He Y. & Deng Y. Design, modeling, and control of morphing aircraft. *Chinese J. Aeronautics*, 2022, **35**(6), 220-246. doi:10.1016/j.cja.2021.09.013
4. Aso, A.; Perrey, M. & Tanaka, H. Experimental study on wing twist-morphing structure using a double-tube cylinder. *Japan Soc. Aeronautical and Space Sci.*, 2017, **15**(a1-a6). doi:10.2322/tastj.15.a1
5. Parker, H.F. The variable camber wing. NACA Report No. 77, 1920.
6. Spillman, J.J. The use of variable camber to reduce drag, weight and costs of transport aircraft. *The Aeronautical J.*, 2016, **96**(951), 1-9. doi:10.1017/S0001924000024404
7. Dhileep, K.; Kumar, D.; Gautham Vigneswar, P.N.; Soni, P.; Ghosh, G.; Ali, S.F. & Arockiarajan, A. Aerodynamic study of single corrugated variable-camber morphing aerofoil concept. *The Aeronautical J.*, 2021, **126**(1296), 316-344. doi:10.1017/aer.2021.71
8. Woods, B.K.S. & Friswell, M.I. Preliminary investigation of a fishbone active camber concept, ASME 2012 Conference on Smart Materials, Adaptive Structures and Intelligent Systems, *SMASIS,* 2013, pp. 555-563. doi:10.1115/SMASIS2012-8058
9. Kumar, R. & Ghosh, S. Numerical investigation of the trailing edge morphing using corrugated skin at a high reynolds number for NACA 0012 & NACA 64(1)-612 airfoils, AIAA Aviation 2023 forum- Applied Computational Fluid Dynamics III. doi:10.2514/6.2023-4088
10. Jawahar, H.K.; Ai, Q. & Azarpeyvand, M. Experimental and numerical investigation of aerodynamic performance for airfoils with morphed trailing edges. *Renewable Energy*, 2018, **127**(1), 355-367. doi:10.1016/j.renene.2018.04.066
11. Weick, J.A. The effect of multiple fixed slots and a trailing-edge flap on the lift and drag of a Clark Y airfoil. NACA Report No.427, 6, 1933
12. Fawzi, S. & Ali, A. H. Slot design procedure for a NACA 4412 at high angle of attack. *J. Mech. Engine. Res. and Developments*, 2021, **44**(8), 188-203. doi:10.13140/RG.2.2.18732.54402
13. Whitman, N.; Sparks, R.; Ali, S. & Ashworth, J. Experimental investigation of slotted airfoil performance with modified slot configurations. *In* Applied Aerodynamics Conference, 2012. doi:10.2514/6.2006-3481
14. Beyhaghi, S. & Amano, R.S. Parametric study on LE slots used on wind turbine airfoils at various angles of attack. *J. Wind Engine. Industrial Aerodynamics*, 2018, **175**, 43-52. doi:10.1016/j.jweia.2018.01.007
15. Sheldahl, R.E. & Klimas, P.C. Aerodynamic characteristics of seven symmetrical airfoil sections through 180° angle of attack for use in aerodynamic analysis of vertical axis wind turbines. Sandia National Laboratories Energy Report No. SAND-80-2114, 1981. doi:10.2172/6548367

CONTRIBUTORS

Mr Ravi Kumar is currently pursuing a PhD in the Department of Aerospace Engineering at the IIT, Madras, India. His research focuses on the investigation of camber-morphing at both the wing and system levels for applications in low and high-speed flows, utilising Computational Fluid Dynamics (CFD).
For the current study, he has worked on the conceptualisation of the problem, performed numerical simulations, presented the results through plots and tables, drafted the initial version of the manuscript and worked on corrections suggested by the reviewers.

Dr Santanu Ghosh obtained his PhD from North Carolina State University (NCSU), United States of America and working as an Associate professor in the Department of Aerospace Engineering at the IIT, Madras, India.
In the current study, he has provided resources for the study, co-drafted the initial version of the manuscript and edited the final versions pre- and post- review.